# Bleaching Kinetics of Artificial Visual Pigments with Modifications near the Ring−Polyene Chain Connection†

Istvan Szundi,‡ Angel R. de Lera,§ Yolanda Pazos,§ Rosana Alvarez,§ Marco Oliana,|| Mordechai Sheves,|| James W. Lewis,‡ and David S. Kliger*,‡

*Department of Chemistry and Biochemistry, University of California, Santa Cruz, California 95064, Departamento de Química Orgánica, Universidade de Vigo, 36200 Vigo, Spain, and Department of Organic Chemistry, Weizmann Institute of Science, Rehovot 76100, Israel*

*Received July 13, 2001*

ABSTRACT: Absorbance difference spectra were recorded at 20 °C from 30 ns to milliseconds after photolysis of lauryl maltoside suspensions of artificial visual pigments derived from 9-*cis* isomers of 5-ethylretinal, 8,16-methanoretinal (a 6-*s*-*trans*-bicyclic analogue), or 5-demethyl-8-methylretinal. In all three pigments, the earliest intermediate that was detected had the characteristics of a mixture of bathorhodopsin and a blue-shifted intermediate, BSI, which is the first decay product of bathorhodopsin in bovine rhodopsin. The first decays resolved on the nanosecond time scale were the formation of the lumirhodopsin analogues. Subsequent decays were able to be fit with a mechanistic scheme which has been shown to apply to both membrane and detergent suspensions of rhodopsin. Large increases were seen in the amount of metarhodopsin I which appeared after photolysis of 5-ethylisorhodopsin and the bicyclic isorhodopsin analogue, while 5-demethyl-8-methylisorhodopsin more closely followed native rhodopsin in decaying through meta $I_{380}$, a 380 nm absorbing precursor to metarhodopsin II. In addition to forming more metarhodopsin I, the bicyclic analogue stabilized the metarhodopsin I−metarhodopsin II equilibrium similarly to what has been previously reported for 9-demethylrhodopsin in detergent, introducing the possibility that the bicyclic analogue could similarly be defective in transducin activation. These observations support the idea that long after initial photolysis, structural details of the retinylidene chromophore continue to play a decisive role in processes leading to the activated form, metarhodopsin II.

The initial action of light on the vertebrate visual pigment rhodopsin is confined to the chromophore, a protonated retinylidene Schiff base (*1*). Subsequent conformational changes of the chromophore trigger a series of transitions within the protein which culminate in the specific modifications to rhodopsin's cytoplasmic surface which activate the G-protein, transducin (*2*). These changes, including deprotonation of the SB,[1] reorganization of several cytoplasmic loops, and proton uptake mediated by Glu-134 (*3*), are not trivial to rationalize because the chromophore binds to a site closer to the opposite, intradiscal surface of the protein (*4, 5*).

A number of intermediates in this activation sequence have been characterized by absorbance spectrophotometry. Several can be trapped at low temperatures, and these as well as an equal number of others have been observed in time-resolved absorbance measurements conducted at physiologically relevant temperatures. Artificial visual pigments, produced by regeneration of the apoprotein opsin with synthetic analogues of retinal, have been used to study the chromophore's role in activation. This approach was initially used to study the earliest intermediates (up to lumirhodopsin, Lumi), which are those most obviously connected with chromophore properties (*6, 7*) and whose kinetics are unaffected by detergent solubilization of rhodopsin. However, besides changes in these early intermediates, work by the Yoshizawa group (*8*) using low-temperature spectroscopy also found changes in the transition temperatures and $\lambda_{max}$ values of the later intermediates of 13-demethylisorhodopsin, and more recently, significant changes in the equilibria of the late intermediates of 9-demethylrhodopsin have been elucidated (*9, 10*). Given that in the latter studies 9-demethylation overwhelmed the effect of detergent solubilization and that detergent effects on the late intermediate kinetic scheme are now better understood (*11*), conditions seem favorable for extending kinetic studies to the late intermediates of more artificial visual pigments. Work has already been reported integrating study of artificial pigments with complementary rhodopsin mutations using transducin activation as an assay (*12*), and studies such as those would benefit greatly from a better

† This work was supported by Grant EY00983 from the National Eye Institute of the National Institutes of Health (to D.S.K.), the Spanish Ministry of Education and Culture (CICYT, Grant SAF98 0143) and Xunta de Galicia (Grant PGIDT99 PXI30105B) (to A.R.d.L.), the AMN Fund for the Promotion of Science, Culture and Arts in Israel (to M.S.), and the Fund for Basic Research (administered by the Israel Academy of Sciences and Humanities) (to M.S.).

‡ University of California.
§ Universidade de Vigo.
|| Weizmann Institute of Science.

[1] Abbreviations: Batho, bathorhodopsin; BSI, blue-shifted intermediate; DIBAL, diisobutylaluminum hydride; fwhm, full width at half-maximum; LDA, lithium diisopropylamide; LM, lauryl maltoside; Lumi, lumirhodopsin; Meta, metarhodopsin; ROS, rod outer segment; SB, Schiff base.

10.1021/bi011461f CCC: $22.00 
Published on Web 01/17/2002

understanding of the late intermediates of artificial pigments in detergent suspensions. Here we report time-resolved measurements of the late intermediates of pigments derived from 9-*cis*-5-ethylretinal, 9-*cis*-8,16-methanoretinal (a bicyclic retinal analogue), and 9-*cis*-5-demethyl-8-methylretinal.

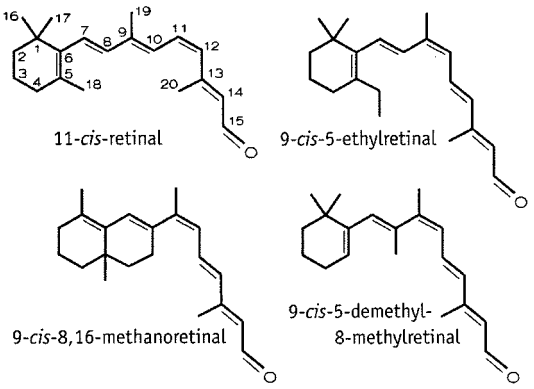


These retinal analogues involve modifications in the vicinity of the ring−chain connection, a region of the chromophore which has been shown previously to be important for the stability of early rhodopsin photointermediates (*7*, *13*). Steric hindrance in the vicinity of the C6−C7 bond has been implicated in control of the decay rate of bathorhodopsin, and this factor should be affected in both 5-ethylisorhodopsin and 5-demethyl-8-methylisorhodopsin. Even stronger constraints on rotation about the C6−C7 bond are imposed in the bicyclic isorhodopsin analogue.

## MATERIALS AND METHODS

*Preparation of Retinal Analogues.* 9-*cis*-8,16-Methanoretinal and 9-*cis*-5-demethyl-8-methylretinal were prepared in high yields (99 and 84%, respectively) by reduction of the retinoic ester analogues using DIBAL in THF, followed by oxidation of the corresponding retinol analogues with $MnO_2$ in the presence of sodium carbonate in $CH_2Cl_2$ (R. Alvarez, Y. Pazos, A. R. de Lera, submitted for publication). The precursor ethyl 9-*cis*-8,16-methanoretinoate was synthesized as previously described (*14*). The precursor ethyl 9-*cis*-5-demethyl-8-methylretinoate was prepared by the stepwise strategy successfully applied to the synthesis of the parent ethyl 9-*cis*-retinoate (*15*).

9-*cis*-5-Ethylretinal was synthesized from 6-methyl-5-hepten-2-one that was converted to its Schiff base by reaction with aniline. Alkylation of its anion (formed by reaction with LDA) with methyl iodide, followed by hydrolysis, gave 7-methyl-6-octen-3-one. Reaction with the sodium salt of diethyl (cyanomethyl) phosphonate followed by reduction with DIBAL gave 3-ethyl-7-methyl-2-octen-1-al. The latter was condensed with acetone followed by cyclization in the presence of $H_2SO_4$ to give 5-ethyl-$\beta$-ionone. This compound was transformed to 9-*cis*-5-ethylretinal by known methods.

The 9-*cis*-retinal analogues were purified by HPLC (Prep Nova Pack HR, silica, 60 Å, 6 $\mu$m, 300 mm × 19 mm; 5% hexane/EtOAC; 5 mL/min) after their preparation following the stereoselective procedures described above. NMR spectra were compared with that of 9-*cis*-retinal, the chemical shift of H10 being particularly diagnostic of the 9-*cis* configuration. In addition, that geometry in analogue 9-*cis*-5-demethyl-8-methylretinal was confirmed by NOE experiments. The NMR spectrum of 9-*cis*-5-ethylretinal was identical to published data (*16*).

*Preparation of Artificial Rhodopsins.* Rod outer segments (ROS) containing bovine opsin were prepared for regenerations as described previously (*13*). Subsequent steps were conducted under dim red light. Regenerations of artificial visual pigments were begun by adding an aliquot of a concentrated chromophore stock solution (freshly prepared in ethanol) to a ROS suspension of opsin. The amount added was sufficient to give a 2−3-fold excess of chromophore over opsin and small enough that ethanol remained less than 3% of the resulting solution. Regenerating mixtures were incubated in the dark at 37 °C, and aliquots were withdrawn periodically to measure the extent of regeneration spectrophotometrically after dilution in 1% Ammonyx LO detergent. While 5-ethylisorhodpsin was stable in Ammonyx LO, the bicyclic isorhodopsin analogue and 5-demethyl-8-methylisorhodopsin decomposed in that detergent with room temperature half-lives of 6 and 4 min, respectively. Somewhat better stability was achieved in octyl glucoside suspensions, but the highest stability was observed using lauryl maltoside, where both pigments were stable even in the presence of 5 mM hydroxylamine. Yields of pigments (based on opsin) were ∼20% for 5-ethylisorhodopsin and 5-demethyl-8-methylisorhodopsin, and ∼50% for the bicyclic isorhodopsin analogue. After regeneration ceased to progress, excess chromophore was converted to the alcohol form by adding 0.1 mg of NADPH (the cofactor for the endogenous ROS retinol dehydrogenase) per milligram of opsin and continuing the incubation for 1 h. Regenerated ROS were stripped of extrinsic membrane proteins by two cycles of centrifugation (Sorvall SS-34 rotor, 30 min at 17K rpm) followed by resuspension in 1 mM EDTA (pH 7.0). After the final wash, membranes were pelleted and the artificial visual pigments were solubilized in sufficient lauryl maltoside detergent in buffer [2% for 5-ethylisorhodpsin and 0.5% for the other pigments (pH 7.0), 10 mM TRIS, 60 mM KCl, 30 mM NaCl, 2 mM $MgCl_2$, and 0.1 mM EDTA] to produce solutions whose absorbance was ∼0.6 (path length of 1 cm) at the peak of the long wavelength pigment absorption band (484 nm for 5-ethylisorhodopsin, 475 nm for the bicyclic isorhodopsin analogue, and 450 nm for 5-demethyl-8-methylisorhodopsin). These pigment $\lambda_{max}$ values were determined from the difference spectra obtained after bleaching an aliquot containing either Ammonyx LO (5-ethylisorhodopsin) or 5 mM hydroxylamine (the other two pigments) with light from a microscope illuminator equipped with a yellow filter. Detergent suspensions of pigments were centrifuged immediately prior to measurements to remove any unsolubilized material.

*Time-Resolved Spectroscopy.* Individual samples were photolyzed by 7 ns (fwhm) laser pulses. The changes in absorbance at particular time delays after photolysis, ranging from 30 ns to tens of milliseconds, were measured using a gated optical multichannel analyzer (*17*). Samples were excited using 477 nm light from a dye laser pumped by the 355 nm third harmonic of a Nd:YAG laser. The flux of energy delivered to the sample was 80 $\mu$J/mm$^2$. Absorbance changes due to rotational diffusion were eliminated by probing with light linearly polarized at 54.7° relative to the laser polarization axis. The path length for probe light in the sample was 2 mm, and sample temperatures were

Scheme 1

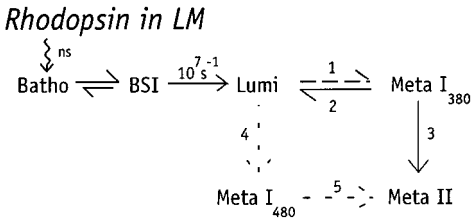


maintained at 20 °C. Fresh sample was pumped into the optical path from a computer-controlled syringe after each photolysis pulse. The spectrum of the pigment bleached by the laser was determined using methods similar to those described previously (*18*).

*Data Analysis.* The sets of experimental difference spectra were fit as previously described (*19*) to a function whose form was a sum of exponential decays:

$$\Delta A(\lambda,t) = b_0(\lambda) + b_1(\lambda)\exp(-t/\tau_1) + b_2(\lambda)\exp(-t/\tau_2) + \ldots$$

The apparent lifetimes ($\tau_i$) and the spectral changes associated with the individual lifetimes, or *b*-spectra [$b_i(\lambda)$], were determined for fits involving up to five exponential terms. The residuals (difference between the fit and data as a function of wavelength) from fits with different numbers of exponentials were compared to determine the best choice using as criteria the spectral structure of residuals relative to the noise level and reproducibility of the fit. Fitting of exponentials does not uniquely determine the mechanistic scheme connecting photointermediates. For example, after photolysis of rhodopsin, five exponential decays are seen on the time scale studied here. The mechanistic scheme which has been determined for native rhodopsin (Scheme 1)[2] was only determined after consideration of a large number of alternatives (*20*). To deduce the scheme that followed, advantage had to be taken of knowledge of the spectrum of the photopigment bleached by the laser, and reasonable assumptions had to be made about the spectral characteristics of photointermediates. These spectra, like those of visual pigments themselves, typically have broad wavelength profiles with roughly Gaussian shape (the red halves of the long wavelength absorption bands of rhodopsin, isorhodopsin, Batho, and Lumi are very well represented by Gaussians), and this character was used to deduce the presence of equilibria and to estimate the equilibrium constants that are involved. Scheme 1 and its associated equilibria have been confirmed using appropriate temperature studies and, with appropriate changes in microscopic rates, have been found to describe rhodopsin both in membrane and in detergent. Schemes similar to Scheme 1 were fit to the data for the artificial pigments studied here, and microscopic rates and intermediate spectra were determined for each pigment. Advantage was taken of the fact that when linear subsets of Scheme 1 are modeled by straight sequences, spectra of intermediates can be directly calculated. If significant back reactions are actually present, the straight sequential intermediates so calculated may represent a mixture of the resolved intermediates which appear in Scheme 1, as indicated by one or more of the straight sequential intermediate spectra deviating from Gaussian character. This characteristic can be used to detect the presence of equilibria and to estimate the equilibrium constants that are involved. Names of intermediates for the artificial pigments are given by reference to the corresponding intermediate which occurs in the native rhodopsin scheme. As a consequence, spectral designations which are part of the names of native rhodopsin intermediates are names only and may not be quantitatively correct for artificial pigment intermediates.

[2] Beginning with decay of the Lumi intermediate, schemes are drawn so that the weight of an arrow is proportional to the magnitude of the rate constant represented by the arrow. Numbers above the arrows give the decay rate for BSI.

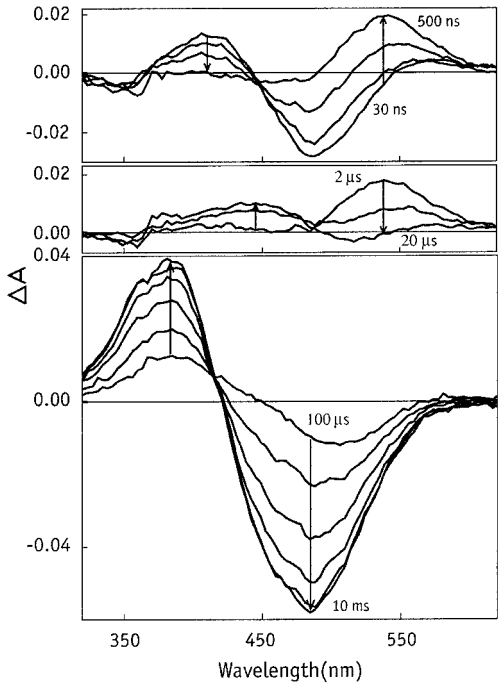


FIGURE 1: Absorbance changes occurring after 477 nm photoexcitation of 5-ethylisorhodopsin at 20 °C. (Top) Absorbance difference spectra collected 30, 60, 90, and 500 ns after the 7 ns photoexcitation pulse. Arrows show the direction of the time-dependent changes in absorbance. (Middle) Absorbance difference spectra collected after delays of 2, 8, and 20 $\mu$s. (Bottom) Absorbance difference spectra collected after delays of 100 $\mu$s, 200 $\mu$s, 400 $\mu$s, 800 $\mu$s, 1 ms, and 10 ms. Data are only shown in separate panels for clarity; all were collected under the same conditions during the same experiment.

## RESULTS

The absorbance difference spectra collected after photolysis of 5-ethylisorhodopsin are shown in Figure 1. The earliest data on the nanosecond time scale (top panel) show decay of a blue-shifted species (relative to the pigment) which decays to a red-shifted product. This behavior contrasts with what is seen in native rhodopsin where on this time scale, the initial red-shifted photoproduct, bathorhodopsin (Batho), decays through a blue-shifted intermediate (BSI) to form lumirhodopsin (Lumi). As is the case for a number of other artificial pigments (*7*, *21*), 5-ethyl-Batho decays into equilibrium with its BSI prior to our first, 30 ns time point. The kinetics seen in the top panel of Figure 1 reflect the decay of the equilibrated mixture to form Lumi. Subsequently (middle panel), Lumi decays on the microsecond time scale to form another blue-shifted product which continues to have the spectrum of a protonated Schiff base, and finally (bottom

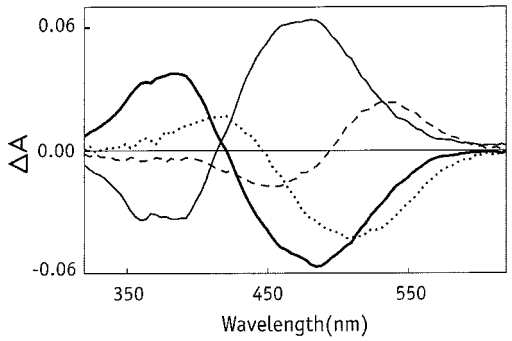


FIGURE 2: *b*-Spectra associated with the three-exponential fit to the data in Figure 1. The dotted, dashed, and thin lines show the absorbance changes associated with the 130 ns, 7.8 $\mu$s, and 330 $\mu$s components, respectively. The thick line shows $b_0$, the time-independent component.

Scheme 2

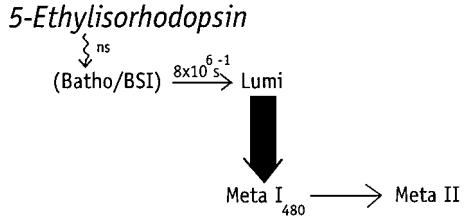


panel), this late protonated Schiff base intermediate decays to a deprotonated Schiff base. A good fit to these data was obtained with three exponential components having apparent lifetimes (130 ns, 7.8 $\mu$s, and 330 $\mu$s). These lifetimes and the associated *b*-spectra shown in Figure 2 could be fit to a portion of the scheme obtained for native rhodopsin (Scheme 2). The spectra of intermediates occurring in such a sequential scheme can be simply calculated from the *b*-spectra (and the spectrum of the bleached pigment) using the apparent rates. The spectra of the straight sequential intermediate are shown in Figure 3. The last two of these spectra correspond to analogous Scheme 1 intermediates, and the first straight sequential intermediate's spectrum corresponds to that of an equilibrated mixture of Batho and BSI. This latter character is supported by the spectrum's deviation from a Gaussian shape with significant tailing to the red, which indicates that this mixture must be resolved into two analogous intermediates from Scheme 1. The Batho−BSI equilibrium constant is clearly forward shifted with the equilibrium constant estimated to be ~7. The $\lambda_{max}$ values of the intermediates from Scheme 2 are given in Table 1, and the microscopic rates are given in Table 2. Four exponential terms could also fit the 5-ethylisorhodopsin photolysis data, but the improvement in residuals was not compelling. Division of the slowest component of the three-exponential fit into two components would imply a mechanism which is not a subset of the native rhodopsin scheme; i.e., it would require a new protonated Schiff base intermediate. Since the grounds for such a new intermediate are weak, the scheme based on the three-exponential fit was adopted, and in any event, it preserves the most distinctive feature of the four-exponential scheme in having a long-lived (compared to detergent-solubilized native rhodopsin) protonated Schiff base intermediate. Evidence for the appearance of metarhodopsin I (Meta $I_{480}$) in this detergent-solubilized sample is strong, as shown by the second *b*-spectrum in Figure 2 (dashed line).

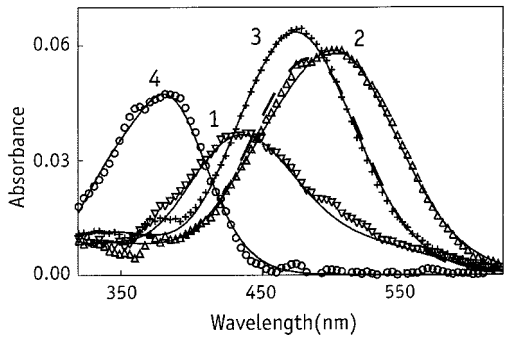


FIGURE 3: Absolute spectra of intermediates which result from fitting the data of Figure 1 to a straight sequential (no back reactions) scheme. Because back reactions are not considered in this fit, the spectrum resulting for the first intermediate (▽) is a mixture of BSI and Batho, accounting for the tailing seen on its red edge. Plotted points compare the data to the fit (smooth lines). Fitted curves were calculated using Scheme 2 with the spectra of the resolved intermediates ($\lambda_{max}$ values given in Table 1) and rate constants (Table 2). The second intermediate (△) corresponds to Lumi, the third (+) to Meta $I_{480}$, and the fourth (○) to Meta II. The dashed line shows the spectrum of the bleach determined from a single laser pulse.

Absorbance difference spectra collected after photolysis of the bicyclic isorhodopsin analogue are shown in Figure 4. The data on the sub-microsecond time scale (top panel) show initial formation of a very red-shifted product, but assignment of this to Batho is inconsistent with the fact that the decay product of this photointermediate is not blue-shifted, but rather has a $\lambda_{max}$ similar to that of its predecessor and a larger extinction coefficient [see Figure 5 (•••)]. Since similar behavior was encountered after photolysis of 5-demethyl-8-methylisorhodopsin on this time scale (see Figure 7), it seems likely that a common feature contributes to the unusual appearance of the early data. Both of these pigments have very blue-shifted absorption spectra for chromophores containing six retinylidene double bonds. In both cases, substitution at the C8 position prevents planarity of 9-*cis* isomers of these retinal analogues in a manner similar to the way that the C13-methyl prevents planarity of 11-*cis* isomers. Such a twist away from planarity reduces conjugation and thus contributes to a blue shift of the pigment spectra. Besides blue shifting the pigment spectra, hindrance in the 9-*cis* isomers of these two pigments also promotes formation of the 11-*cis* isomer via secondary photolysis, relative to the unhindered rhodopsin case. Evidence for this comes from the fact that for both hindered pigments the bleach spectrum measured using the laser pulse was approximately 10 nm blue-shifted relative to the bleach measured using nonlaser light. In the case of unhindered 5-ethylisorhodopsin, these two measurements agreed within 1 nm, showing little conversion there of 9-*cis* to 11-*cis* by the laser pulse, similar to what occurs for native rhodopsin when excited at 477 nm. Therefore, secondary photolysis further blue shifts the bleaching portion of the difference spectra and acts in tandem with the already blue-shifted spectra of these hindered 9-*cis* pigments to make even a normal BSI seem red shifted. In fact, the observed increase in the extinction coefficient seen on the sub-microsecond time scale after photolysis of the bicyclic isorhodopsin analogue is consistent with the usual spectral behavior of a BSI converting into its Lumi (*7*). Subsequent difference spectra (Figure 4, bottom panel) show decay of Lumi to form

Table 1: Spectra of Intermediates Determined from Fitting Scheme 1 to Absorption Difference Spectra

| | 5-ethylisorhodopsin | bicyclic isorhodopsin analogue | 5-demethyl-8-methylisorhodopsin | rhodopsin | isorhodopsin |
|---|---|---|---|---|---|
| Batho | 532 nm | 532 nm | 523 nm | 531 nm[a] | 525 nm[b] |
| BSI | 435 nm | 474 nm | 438 nm | 473 nm[a] | 483 nm[b] |
| Lumi | 500 nm | 518 nm | 469 nm | 493 nm[c] | 487 nm[b] |
| Meta $I_{480}$ | 473 nm | 534 nm | – | 486 nm[c] | *d* |
| Meta $I_{380}$ | – | – | 370 nm | 377 nm[c] | *d* |
| Meta II | 380 nm | 406 nm | 370 nm | 377 nm[c] | *d* |
| Bleach[e] | 483 nm | 464 nm | 440 nm | 500 nm[c] | 483 nm[b] |

[a] Data at 22 °C from Hug et al. (*19*). [b] Data at 20 °C from Lewis et al. (*22*). [c] Data at 22 °C from Mah et al. (*29*). [d] Late intermediates formed after isorhodopsin photolysis have not been characterized under conditions comparable to those studied here. [e] Determined from the pigment bleached by one laser pulse.

Table 2: Microscopic Rate Constants Determined from Fitting Schemes to Absorption Difference Spectra

| | 5-ethyliso-rhodopsin | bicyclic isorhodopsin analogue | 5-demethyl-8-methylisorhodopsin | rhodopsin[a] |
|---|---|---|---|---|
| $k_1$ ($s^{-1}$)[b] | – | – | 4100 | 2500 |
| $k_2$ ($s^{-1}$) | – | – | 3000 | 3200 |
| $k_3$ ($s^{-1}$) | – | – | 1100 | 3000 |
| $k_4$ ($s^{-1}$) | 130000 | 38000 | – | 470 |
| $k_5$ ($s^{-1}$) | 3000 | 7700 | – | 550 |
| $k_6$ ($s^{-1}$) | – | 3200 | – | 40 |

[a] Data at 22 °C from Mah et al. (*29*). [b] Estimated microscopic rate constants for BSI decay are shown on the schemes.

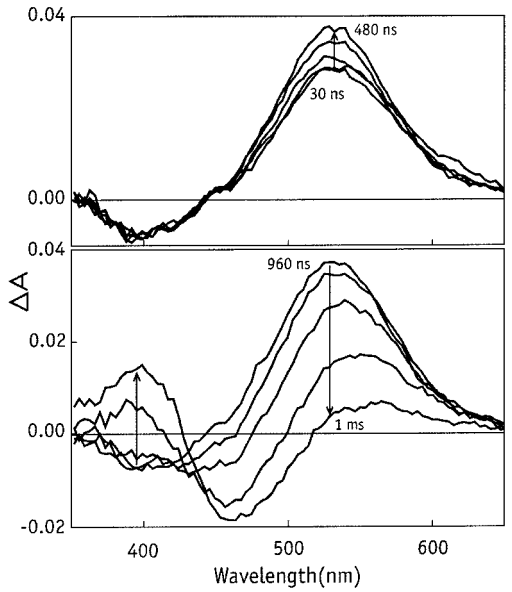


FIGURE 4: Absorbance changes occurring after 477 nm photoexcitation of the bicyclic isorhodopsin analogue at 20 °C. (Top) Absorbance difference spectra collected 30, 60, 120, 240, and 480 ns after the 7 ns photoexcitation pulse. The arrow shows the direction of the time-dependent changes in absorbance. (Bottom) Absorbance difference spectra collected after delays of 0.96, 10, 30, 100, and 1 ms. A limited amount of additional data collected at 10 ms showed that no further changes occur after 1 ms (not shown).

deprotonated Schiff base products. The data were best fit by three exponentials with apparent lifetimes of 220 ns, 27 $\mu$s, and 90 $\mu$s. Residuals present in both the 30 and 60 ns times were consistent with the tail of a fast Batho−BSI transition possibly being present but unresolved in the three-exponential fit. The lifetimes and the associated *b*-spectra shown in Figure 5 could be fit to a portion of the scheme derived for native rhodopsin (Scheme 3). The straight

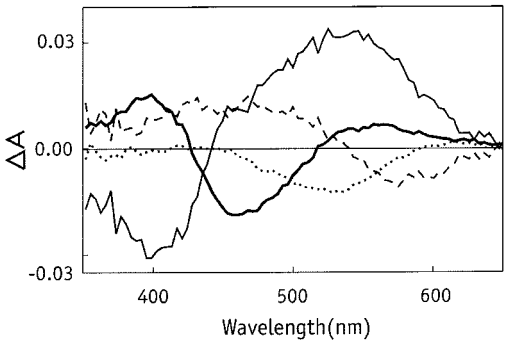


FIGURE 5: *b*-Spectra associated with the three-exponential fit to the data in Figure 4. The dotted, dashed, and thin lines show the absorbance changes associated with the 220 ns, 27 $\mu$s, and 92 $\mu$s components, respectively. The thick line shows $b_0$, the time-independent component.

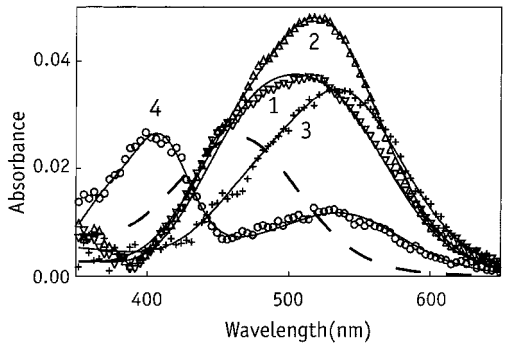


FIGURE 6: Absolute spectra of intermediates which result from fitting the data of Figure 4 to a straight sequential scheme. Like the 5-ethylisorhodopsin case in Figure 3, the spectrum resulting for the first intermediate (▽) is a mixture of BSI and Batho, accounting for the tailing seen on its red edge. The fourth and final intermediate (○) also corresponds to an equilibrated mixture (Meta $I_{480}$ and Meta II). Plotted points compare the data to the fit (smooth lines). Fitted curves were calculated using Scheme 3 with the spectra of the resolved intermediates ($\lambda_{max}$ values given in Table 1) and rate constants (Table 2). The second intermediate (△) corresponds to Lumi, and the third (+) corresponds to Meta $I_{480}$. The dashed line shows the spectrum of the bleach determined from a single laser pulse.

sequential intermediates produced by fitting the data are shown in Figure 6. There, two of the straight sequential intermediates are equilibrated mixtures of Scheme 1 intermediates. The spectra can be resolved into a set of intermediates analogous to those of Scheme 1, the $\lambda_{max}$ values of which are given in Table 1. The Batho−BSI equilibrium for the bicyclic analogue was not forward shifted (equilibrium constant estimated to be ~0.7). The microscopic rates determined for Scheme 3 are given in Table 2. Note that Scheme 3 contains a back reaction from Meta II to Meta

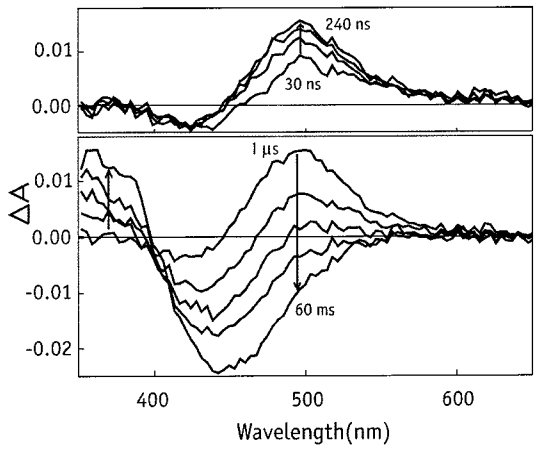


FIGURE 7: Absorbance changes occurring after 477 nm photoexcitation of the 5-demethyl-8-methylisorhodopsin at 20 °C. (Top) Absorbance difference spectra collected 30, 60, 120, and 240 ns after the 7 ns photoexcitation pulse. The arrow shows the direction of the time-dependent changes in absorbance. (Bottom) Absorbance difference spectra collected after delays of 1 $\mu$s, 100 $\mu$s, 300 $\mu$s, 1 ms, and 60 ms.

Scheme 3

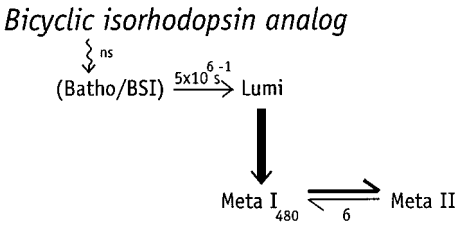


$I_{480}$ which is normally insignificant for detergent-solubilized native rhodopsin. However, that change does not represent a deviation from the native rhodopsin scheme since that back reaction occurs prominently in the scheme followed by membrane suspensions of rhodopsin.

As discussed above, the data for 5-demethyl-8-methylisorhodopsin at early times is similar to that for the bicyclic isorhodopsin analogue, and analysis in terms of a rapidly formed (<30 ns) equilibrated mixture of Batho and BSI is supported by the shape of the first straight sequential intermediate shown in Figure 8. The spectra shown there were obtained from the best fit to the data in Figure 7 which found three exponentials with lifetimes of 45 ns, 130 $\mu$s, and 1.7 ms. Here, as was the case for the bicyclic isorhodopsin analogue, two straight sequential intermediates are clearly mixtures of Scheme 1 intermediates, but now the first and second sequential intermediates are equilibrated mixtures, whereas for the bicyclic isorhodopsin analogue, mixtures occurred for the first and third. Thus, this artificial pigment follows a different portion of the native rhodopsin scheme (Scheme 4) than the other two artificial pigments do. The Batho−BSI equilibrium was the most forward shifted of the pigments studied here with an equilibrium constant estimated to be ~9. Again, the $\lambda_{max}$ values of the 5-demethyl-8-methylisorhodopsin intermediates corresponding to Scheme 1 are given in Table 1, and the microscopic rates determined for Scheme 4 are given in Table 2.

## DISCUSSION

*Early Photolysis Intermediates.* All three of the artificial visual pigments studied here have relatively unstable Batho

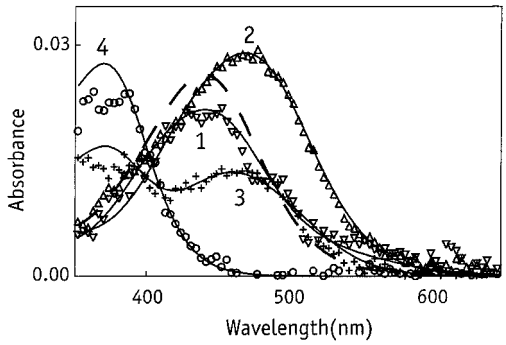


FIGURE 8: Absolute spectra of intermediates which result from fitting the data of Figure 7 to a straight sequential scheme. As was the case for the other artificial pigments studied here, the spectrum resulting for the first intermediate (▽) is a mixture of BSI and Batho, accounting for the tailing seen on its red edge. The third intermediate (+) also corresponds to an equilibrated mixture (Lumi and Meta $I_{380}$). Plotted points compare the data to the fit (smooth lines). Fitted curves were calculated using Scheme 4 with the spectra of the resolved intermediates ($\lambda_{max}$ values given in Table 1) and rate constants (Table 2). The second intermediate (△) corresponds to Lumi, and the fourth (○) corresponds to Meta II. The dashed line shows the spectrum of the bleach determined from a single laser pulse.

Scheme 4

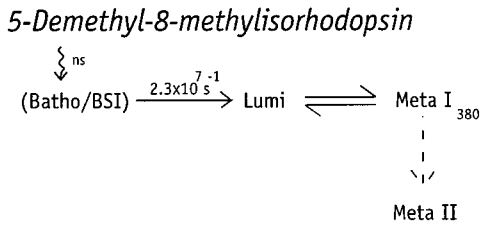


intermediates whose decay was essentially complete at the first time point that was studied (30 ns). While 5-ethylisorhodopsin and 5-demethyl-8-methylisorhodopsin displayed very forward shifted Batho−BSI equilibria, and hence fall into the pattern of a number of other artificial pigments which have fast BSI formation, the bicyclic analogue was unusual in having a somewhat back-shifted Batho−BSI equilibrium. The idea that the bicyclic Batho was more stable relative to its BSI than those of the other artificial pigments is supported by the fact that its residuals at 30 and 60 ns indicated that the tail of the Batho decay may have been captured but not resolved in the three-exponential fit. The observed back-shifted Batho−BSI equilibrium is similar to what was observed in several other artificial visual pigments with chromophores which increased the steric bulk along the polyene chain (*13*), as is also the case for the bicyclic chromophore. One way such an effect on the equilibrium could arise is if BSI formation involved movement of the polyene chain into a more restrictive cleft in the protein with which extra bulk interfered. Another possible explanation is that the extra bulk along the chain constrains torsional modes of the polyene chain. The movement of the energy of several such torsional modes from above *kT* in Batho to below *kT* in BSI is believed to account for the entropic driving force toward BSI (*23*).

The pattern of the BSI $\lambda_{max}$ values is of interest since it has been proposed that torsion of the C6−C7 bond away from planarity reduces the level of conjugation, contributing to BSI's blue shift (*24*). Here, in the bicyclic analogue where such torsion is constrained, the BSI has little or no blue shift

(relative to its parent pigment), while for the other two pigments, the BSI shows substantial blue shifts. Previously, Shichida and co-workers studied two 6-*s*-*cis*-locked bicyclic artificial pigments with five- and seven-membered locking rings, 6,5-rhodopsin and 6,7-rhodopsin, respectively (*25*). In those low-temperature studies, the 6,7-rhodopsin exhibited a less stable Batho which decayed through a BL intermediate whose $\lambda_{max}$ was near 495 nm. Since we believe BL corresponds to a mixture of Batho and BSI which is similar to the first of our time-resolved straight sequential intermediates in Figure 6, there seems to be at least qualitative agreement in the behavior of these two pigments. That was somewhat surprising given that 6,7-rhodopsin was a locked 6-*s*-*cis* pigment while our bicyclic pigment is a locked 6-*s*-*trans* species. However, this may be explained by the six-membered locking ring creating a more planar 6-*s*-*trans* species which coincides roughly in spectrum with a more twisted 6-*s*-*cis* species locked by the seven-membered ring. The relatively red-shifted spectrum of the Lumi intermediates in both pigments supports the idea that the difference in 6-*s* character may be compensated by differences in C5═C6−C7═C8 planarity. The magnitude of the locking ring size effect is demonstrated by the fact that the Batho of 6,5-rhodopsin occurs at ∼555 nm while that of 6,7-rhodopsin occurs at ∼505 nm (*25*). Thus, the twisting effect of a single extra carbon in the locking ring (∼25 nm) is on the same order of magnitude as the 20 nm difference in protonated Schiff base $\lambda_{max}$ values between locked 6-*s*-*cis* and locked 6-*s*-*trans* isomers of 8,16-methanoretinal (*26*).

*Kinetic Changes in the Late Photolysis Intermediates.* Although the initial stages of protein change have begun at Lumi, subsequent intermediates become more closely associated with activation as the reaction proceeds toward the final proton uptake following Meta II formation (*11*), making these later intermediates of great significance to transduction. However, despite the intrinsic interest, knowledge of an intermediate's character depends critically on a detailed understanding of its predecessor. While a good deal is known about the more constrained early photointermediates, fewer artificial pigment studies have been directed at the later intermediates, placing the current work in a much less developed context. Counterbalancing this are recent advances such as the rhodopsin X-ray structure (*5*) and temperature-resolved photoaffinity labeling of rhodopsin (*27*) which put the interpretation of events after Lumi on an improved foundation.

The greatest change in the Lumi decay rate in these artificial pigments from what has been observed in native rhodopsin was seen after photolysis of 5-ethylisorhodopsin. Extension of the C5 methyl to an ethyl group dramatically increased the rate of formation of Meta $I_{480}$ from Lumi. The acceleration in this rate was so great that the population of Lumi was depleted before the usually dominant Lumi decay route in detergent, through Meta $I_{380}$, proceeds to any significant extent. Even though the subsequent decay of Meta $I_{480}$ is much faster than usual, and its rate is equal to that usually seen for Meta $I_{380}$, the accelerated formation of Meta $I_{480}$ results in a 3-fold net prolongation of the lifetime of the protonated Schiff base after photoexcitation of this artificial pigment. Similar behavior, but to a lesser degree, was observed in the decay of the bicyclic Lumi, which exhibited a smaller increase in the rate of Meta $I_{480}$ formation, but a larger increase in its decay rate. As a result, there was a smaller change in the lifetime of the protonated Schiff base, but clearly, a similar evolution in its environment was present for the bicyclic chromophore as occurs for the 5-ethyl chromophore. A very distinctive feature of the bicyclic pigment's behavior was the formation of a stable Meta $I_{480}$−Meta II equilibrium mixture which presumably decays slowly as the Meta II reacts with the hydroxylamine present in that sample. Similar behavior has been recently reported in another artificial pigment, 9-demethylrhodopsin (*9*, *10*). It is notable that in both cases the chromophore modification was able to overwhelm the effects of the lauryl maltoside detergent, which normally forward shifts the equilibrium completely to Meta II. Parallels in the late intermediates can also be seen between our bicyclic pigment and the previously studied locked 6-*s*-*cis* bicyclic pigment, 6,7-rhodopsin, which similarly displayed a less stable Lumi relative to Meta $I_{480}$ (lower transition temperature) and a back-shifted equilibrium between Meta $I_{480}$ and Meta II compared to what was observed after photoexcitation of native rhodopsin (*25*).

Of the three artificial pigments studied here, 5-demethyl-8-methylisorhodopsin displayed the least perturbed late intermediate scheme. This is perhaps not surprising since this chromophore has the same number of carbon atoms as retinal itself, and the X-ray structure of rhodopsin shows the C5 methyl to be in contact with the C8 hydrogen (*5*), presumably meaning that the exchange of these two groups results in only a small shift of steric bulk within the chromophore, at least in the dark state. The modification may more substantially perturb the chromophore in the late intermediates since it seems to shift the Lumi−Meta $I_{380}$ equilibrium toward Meta $I_{380}$. Subsequent decay of Meta $I_{380}$ to Meta II was slowed, indicating that the artificial chromophore may preferentially stabilize Meta $I_{380}$. It is of interest that a similar pattern of changes occurs in detergent-solubilized rhodopsin which contains a non-native disulfide between cysteines 140 and 222 (*28*). While the X-ray structure shows the C8 substituent pointing away from the base of helix V (which contains Cys-222), rotation of the polyene chain which is presumed to occur during BSI formation (*13*) may position the C8 methyl to interact with the base of that helix or with the end of extracellular loop 2 which leads to it. This could produce a constraint on the motion of helix V, as in the non-native disulfide.

The large perturbations in the late bleaching kinetics seen for all three artificial pigments studied here demonstrate that the chromophore of rhodopsin does not merely trigger early events and then become a passive observer as changes propagate through the protein. Instead, the kinetics of formation and decay of the intermediates following Lumi leading to activation of transducin are controlled by specific structural details of retinal structure. This is particularly clear in the case of 5-ethylisorhodopsin which dramatically facilitates formation of Meta $I_{480}$ relative to the native rhodopsin case. An equally dramatic shift in the Meta $I_{480}$−Meta II equilibrium is seen in the case of the bicyclic isorhodopsin analogue studied here, which has behavior intermediate between that of native rhodopsin and what was recently seen for 9-demethylrhodopsin (*9*). These results are exciting because they apparently demonstrate general control of these late reactions by synthetic modifications of the chromophore. They indicate a more direct influence on Meta

II formation than the more widely studied synthetic retinoid effects seen in electrophysiology which likely reflect changes in Meta II decay (*30*). If a detailed mechanistic understanding can be developed of how synthetic modifications of retinal control Meta II formation, it would be an important step toward opening a way of exercising similar control over other members of the heptahelical G-protein-coupled receptor family using synthetic modification of their ligands.

## ACKNOWLEDGMENT

J.W.L. acknowledges a helpful discussion during the early stages of this work with Dr. Hiroo Imai about his results from a related bicyclic visual pigment.

## REFERENCES

1. Wang, Q., Kochendoerfer, G. G., Schoenlein, R. W., Verdegem, P. J. E., Lugtenburg, J., Mathies, R. A., and Shank, C. V. (1996) *J. Phys. Chem. 100*, 17388−17394.
2. Stryer, L. (1990) *J. Biol. Chem. 266*, 10711−10714.
3. Hofmann, K. P., Jäger, S., and Ernst, O. P. (1995) *Isr. J. Chem. 35*, 339−355.
4. Sakmar, T. P., Franke, R. R., and Khorana, H. G. (1989) *Proc. Natl. Acad. Sci. U.S.A. 86*, 8309−8313.
5. Palczewski, K., Kumasaka, T., Hori, T., Behnke, C. A., Motoshima, H., Fox, B. A., Le Trong, I., Teller, D. C., Okada, T., Stenkamp, R. E., Yamamoto, M., and Miyano, M. (2000) *Science 289*, 739−745.
6. Kropf, A. (1976) *Nature 264*, 92−94.
7. Randall, C. E., Lewis, J. W., Hug, S. J., Björling, S. C., Eisner-Shanas, I., Friedman, N., Ottolenghi, M., Sheves, M., and Kliger, D. S. (1991) *J. Am. Chem. Soc. 113*, 3473−3485.
8. Shichida, Y., Kropf, A., and Yoshizawa, T. (1981) *Biochemistry 20*, 1962−1968.
9. Meyer, C. K., Böhme, M., Ockenfels, A., Gärtner, W., Hofmann, K. P., and Ernst, O. P. (2000) *J. Biol. Chem. 275*, 19713−19718.
10. Vogel, R., Fan, G., Sheves, M., and Siebert, F. (2000) *Biochemistry 39*, 8893−8908.
11. Szundi, I., Mah, T. L., Lewis, J. W., Jäger, S., Ernst, O. P., Hofmann, K. P., and Kliger, D. S. (1998) *Biochemistry 37*, 14237−14244.
12. Han, M., Groesbeek, M., Sakmar, T. P., and Smith, S. O. (1997) *Proc. Natl. Acad. Sci. U.S.A. 94*, 13442−13447.
13. Lewis, J. W., Pinkas, I., Sheves, M., Ottolenghi, M., and Kliger, D. S. (1995) *J. Am. Chem. Soc. 117*, 918−923.
14. Dominguez, B., Pazos, Y., and de Lera, A. R. (2000) *J. Org. Chem. 65*, 5917−5925.
15. Pazos, Y., and de Lera, A. R. (1999) *Tetrahedron Lett. 40*, 8287−8290.
16. Hopf, H., and Krause, N. (1987) *Liebigs Ann. Chem. 1987*, 943−947.
17. Lewis, J. W., and Kliger, D. S. (1993) *Rev. Sci. Instrum. 64*, 2828−2833.
18. Albeck, A., Friedman, N., Ottolenghi, M., Sheves, M., Einterz, C. M., Hug, S. J., Lewis, J. W., and Kliger, D. S. (1989) *Biophys. J. 55*, 233−241.
19. Hug, S. J., Lewis, J. W., Einterz, C. M., Thorgeirsson, T. E., and Kliger, D. S. (1990) *Biochemistry 29*, 1475−1485.
20. Szundi, I., Lewis, J. W., and Kliger, D. S. (1997) *Biophys. J. 73*, 688−702.
21. Mah, T. L., Lewis, J. W., Sheves, M., Ottolenghi, M., and Kliger, D. S. (1995) *Photochem. Photobiol. 62*, 356−360.
22. Lewis, J. W., Liang, J., Ebrey, T. G., Sheves, M., Livnah, N., Kuwata, O., Jäger, S., and Kliger, D. S. (1997) *Biochemistry 36*, 14593−14600.
23. Lewis, J. W., and Kliger, D. S. (1992) *J. Bioenerg. Biomembr. 24*, 201−210.
24. Lewis, J. W., Fan, G.-B., Sheves, M., Szundi, I., and Kliger, D. S. (2001) *J. Am. Chem. Soc. 123*, 10024−10029.
25. Imamoto, Y., Sakai, M., Katsuta, Y., Wada, A., Ito, M., and Shichida, Y. (1996) *Biochemistry 35*, 6257−6262.
26. van der Steen, R., Biesheuvel, P. L., Mathies, R. A., and Lugtenburg, J. (1986) *J. Am. Chem. Soc. 108*, 6410−6411.
27. Borhan, B., Souto, M. L., Imai, H., Shichida, Y., and Nakanishi, K. (2000) *Science 288*, 2209−2212.
28. Lewis, J. W., Szundi, I., and Kliger, D. S. (2000) *Biochemistry 39*, 7851−7855.
29. Mah, T. L., Szundi, I., Lewis, J. W., Jäger, S., and Kliger, D. S. (1998) *Photochem. Photobiol. 68*, 762−770.
30. Corson, D. W., Kefalov, V. J., Cornwall, M. C., and Crouch, R. K. (2000) *J. Gen. Physiol. 116*, 283−297.

BI011461F